

Hexagonal-Pyramid Arrow-Slot Array for Space-based ADS-B

Javier Vera-Sánchez*, Miguel Ferrando-Rocher*, Gorka Casasús-Goyeneche*, Miguel Ferrando-Bataller*

*Antennas and Propagation Lab, iTEAM Research Institute, Universitat Politècnica de València, Spain

{jversan2, miguel.ferrando, jcasgoy, mferrand}@upv.es

Abstract—A compact, fully metallic 4×4 arrow-slot array is proposed as a modular building block for space-based Automatic Dependent Surveillance–Broadcast (ADS-B) reception in Low Earth Orbit (LEO). Each slot is center-fed by a microstrip line, and right-hand circular polarization is achieved through sequential rotation with 90° element orientation and phase progression. Six identical subarrays form a three-dimensional hexagonal-pyramid assembly providing continuous 360° azimuth coverage with beams tilted toward Earth. Full-wave simulations demonstrate excellent impedance matching, low inter-element coupling, and stable radiation characteristics across all faces. The proposed architecture combines the manufacturability and robustness of metal-only slot structures with the polarization control of phased arrays, offering an efficient and low-cost solution for next-generation space-based ADS-B payloads.

Index Terms—ADS-B, air traffic surveillance, arrow-slot arrays, circular polarization, LEO, sequential rotation.

I. INTRODUCTION

Space-based Automatic Dependent Surveillance–Broadcast (ADS-B) extends air-traffic surveillance beyond terrestrial radar, enabling continuous monitoring over oceans and remote areas. This is particularly relevant for European airspace, where maritime routes and sparse ground infrastructure demand wide, low-latency coverage. Space-based ADS-B payloads impose stringent constraints on antenna subsystems: minimal profile, low mass, robustness to the space environment, low manufacturing cost, and high radiation efficiency are necessary to meet satellite mass/volume and power budgets [1].

This work is carried out within the framework of the SATERA project [2], a Horizon Europe initiative aligned with SESAR’s goals to modernise Europe’s aviation Communication, Navigation and Surveillance (CNS) infrastructure under the *Digital European Sky* vision, ensuring the safe and efficient management of airspace through advanced technological solutions, including satellite-based ADS-B systems [3]. SATERA targets reliable aircraft detection over remote and oceanic regions by deploying a constellation of LEO satellites operating around 600 km altitude as illustrated in Fig. 1, which presents the proposed system architecture.

Recent trends for LEO payload antennas include planar phased panels, metasurface and SIW-based arrays, and compact waveguide/slot solutions prioritizing efficiency and mechanical ruggedness for space qualification. These approaches highlight the trade-off between field-of-view control and beam steering on the one hand, and mass, profile, and fabrication

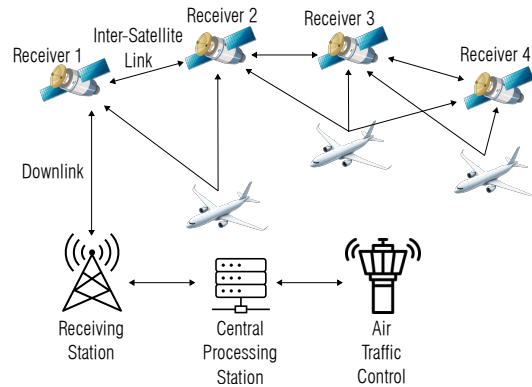
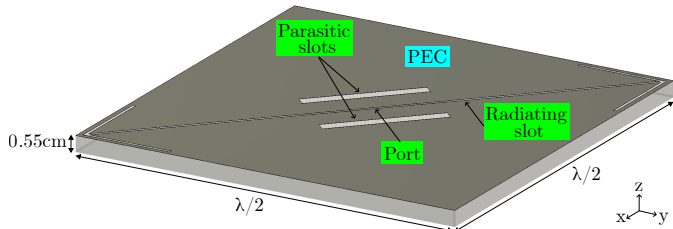


Fig. 1. SATERA system architecture.

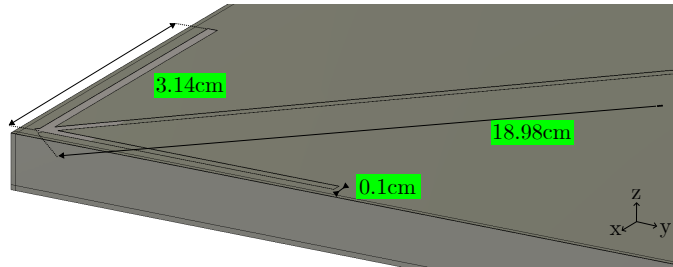
complexity on the other [4], [5]. Slot antennas remain attractive due to low profile, metal-only construction, and good aperture efficiency when backed or properly matched. Current research emphasizes low-loss feeds (e.g., SIW/parallel-plate, cavity backing, differential/series feeds) and geometries/matching stubs that extend bandwidth and shape the pattern [6].

As part of the ongoing antenna development activities within the SATERA project [7], [8], this paper introduces a new array configuration specifically tailored for LEO satellite integration. This work investigates a plane, fully metallic 4×4 arrow-shaped slot array with center microstrip feeding per element. Circular polarization (CP) is realized at the array level via sequential rotation of element orientations and 90° phase progression. A modular 3D hexagonal-pyramid configuration of identical subarrays then provides full 360° azimuthal coverage with beams tilted toward Earth for space-based ADS-B reception. The 24 rows of radiating elements resulting from the 6 faces of the hexagonal pyramid are connected to 24 synchronized digital receivers across multiple satellites, following the synchronization described in [9]. Further details on the SATERA receiver architecture can be found in [10].

Starting from the unit cell, a planar 4×4 subarray is formed, maintaining equal inter-element spacing along both axes. CP is obtained using sequential rotation: the 4×4 is partitioned into 2×2 sectors whose elements are rotated by 90° relative to each other, while the excitation phases are shifted by 90° counterclockwise. The combination of spatial rotation and phase progression yields a right-hand circularly polarized



(a) Unit-cell antenna highlighting the top surface.



(b) Close-up of the arrow end.

Fig. 2. CST model of the proposed arrow-slot unit cell: (a) full view with materials and general dimensions; (b) close-up showing dimensional details.

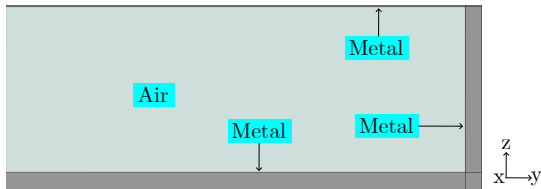


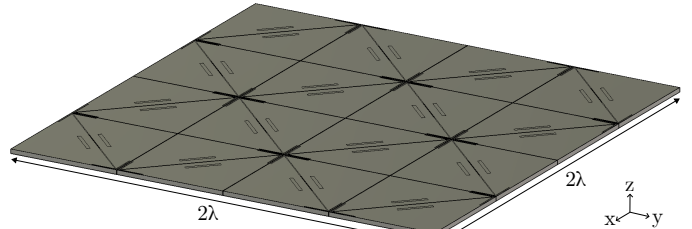
Fig. 3. Side view of the layers that make the unit-cell.

(RHCP) broadside field with uniform amplitude distribution.

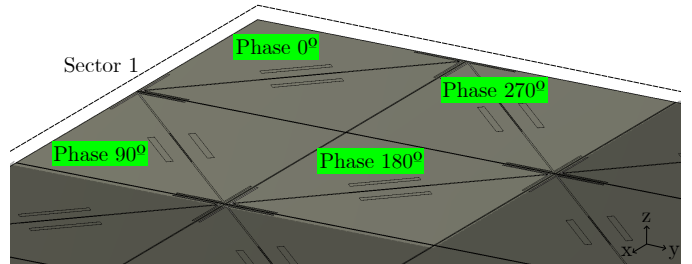
Building upon the 4×4 subarray, a 3D array architecture is devised to provide omnidirectional azimuthal coverage. Six identical planar subarrays are arranged as faces of a hexagonal pyramid around a central axis, each face covering a 60° azimuthal sector ($\pm 30^\circ$). Each face is tilted by 20° with respect to the horizontal plane so that the main beams are directed toward Earth when mounted on a LEO platform. The remainder of this paper describes the antenna architecture, the design of the unit-cell and subarray, and the resulting array performance obtained from full-wave simulations.

II. ANTENNA DESCRIPTION

The radiating element is a cavity-backed slot with an arrow-shaped aperture etched on a metallic ground plane. The unit cell has size $\lambda/2 \times \lambda/2$ at 1090 MHz, with $\lambda = 27.52$ cm, enabling compact replication within the array and promoting broadside radiation with minimal pointing offsets. The arrow topology provides symmetry and an electrically longer aperture than a straight slot of the same footprint. Two tapered appendices are added at the ends of the main diagonal slot (oriented at 45° relative to the x - and y -axes) to extend the effective electrical path without expanding the physical boundaries. The total slot perimeter is 62.17 cm, slightly more than 2λ , which contributes to efficient radiation of the element.



(a) 4×4 array 3D model.



(b) Close-up of sector 1 with phase excitation.

Fig. 4. 4×4 subarray and representative sector illustrating sequential rotation and phase distribution.

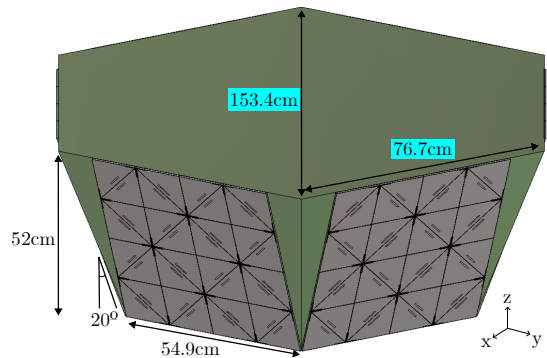


Fig. 5. Perspective view of the 3D hexagonal-pyramid array in CST, with dimensions.

A 12 mm margin to ground-plane edges is maintained to mitigate current crowding and reduce mutual coupling in array operation. Two symmetric parasitic slots surround the main aperture to confine surface currents and to offer an additional degree of freedom for impedance tuning, easing the match to 50Ω .

Excitation is implemented by a microstrip line centered along the slot longitudinal axis. The line width is half the slot width (the slot width is 1 mm), ensuring symmetric coupling. In simulations, a discrete port at the geometric center applies a differential voltage between slot edges. A metallic cavity beneath the ground plane acts as a resonant back structure, redirecting energy toward broadside and improving efficiency; the cavity is air-filled (or vacuum-filled in space) to avoid dielectric losses.

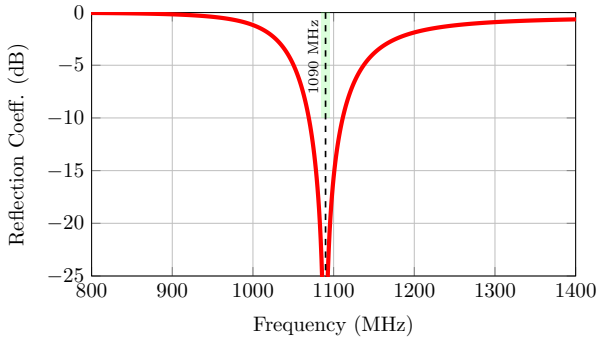


Fig. 6. Return loss of the unit-cell antenna.

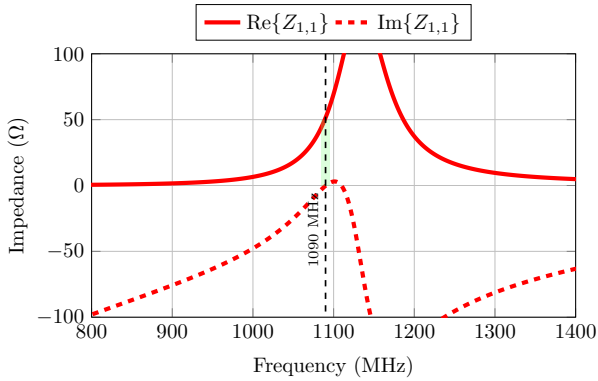


Fig. 7. Input impedance Z_{11} of the unit-cell antenna.

III. SIMULATED RESULTS

The electromagnetic performance of the proposed arrow-shaped slot antenna and its corresponding arrays has been analyzed using full-wave simulations in CST Microwave Studio. The following subsections summarize the main results obtained in terms of impedance matching, mutual coupling, radiation pattern, directivity, and polarization characteristics.

A. Single Element Performance

As shown in Fig. 6, the unit-cell antenna exhibits an excellent impedance matching response, with a return loss better than -25 dB at the design frequency of 1090 MHz. The antenna provides a measured -10 dB bandwidth of approximately 42 MHz, which represents a narrow yet suitable operational range for the ADS-B receiver. Such a bandwidth helps to mitigate the receiver noise figure and therefore contributes to improving the overall signal-to-noise ratio (SNR) and link budget performance of the spaceborne ADS-B system.

The input impedance response, illustrated in Fig. 7, shows a nearly perfect real part close to 50Ω at the operating frequency, with negligible reactive component. This confirms the high-quality impedance tuning achieved through the optimization of the feed position and the inclusion of the parasitic slots. The rapid variation of both resistance and reactance beyond 1090 MHz explains the limited but well-defined operational bandwidth observed in Fig. 6.

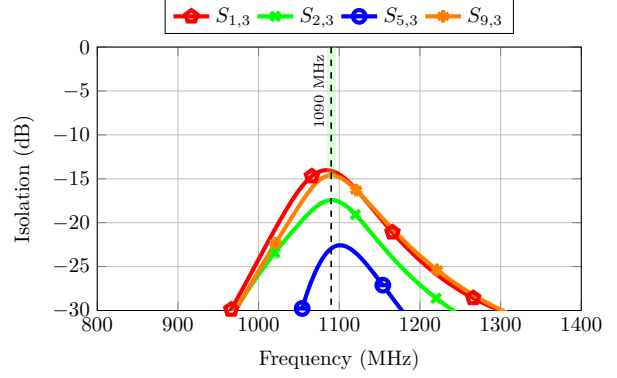


Fig. 8. Inter-element coupling in the 4×4 array.

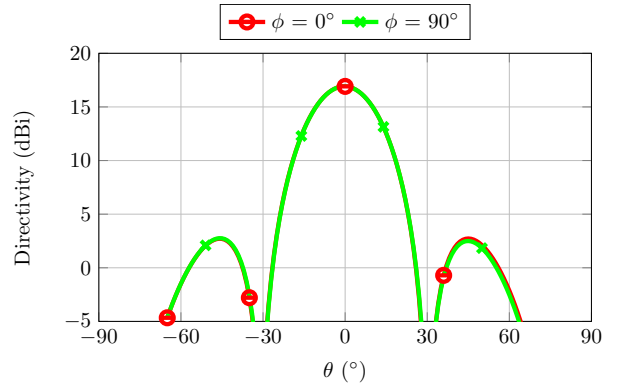


Fig. 9. Co-polar patterns at $\phi = 0^\circ$ and $\phi = 90^\circ$ for the 4×4 array.

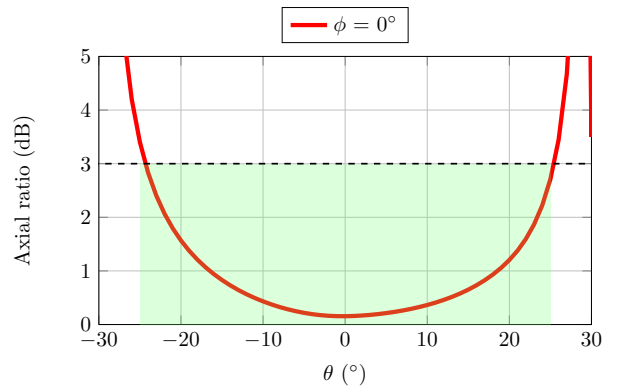


Fig. 10. Axial ratio of the 4×4 array.

B. Planar Array Performance

The 4×4 array designed from the unit-cell element was simulated to evaluate inter-element coupling and array-level radiation characteristics. Figure 8 shows the worst-case coupling curves among selected elements. Even under the least favorable configurations, the coupling remains below -15 dB across the operating band, except for two isolated cases where the limit is slightly exceeded at 1090 MHz. These results confirm that the surface currents are well confined within each unit cell, a consequence of both the cavity-backed configura-

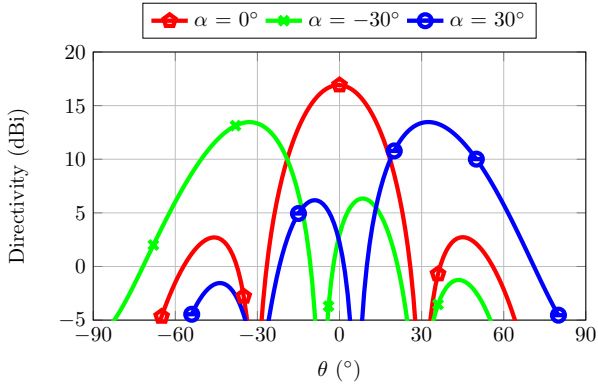


Fig. 11. Beam steering example with three beams in the 4×4 array.

tion and the additional parasitic slots, which effectively reduce undesired interactions between adjacent elements.

The copolar radiation patterns of the 4×4 array are presented in Fig. 9. The main beam points precisely toward the broadside direction, achieving a maximum directivity of 16.91 dBi, total efficiency above 92% and a -3 dB beamwidth of 25.7° . This value is remarkably close to the theoretical upper limit of 17 dBi for a planar aperture of $2\lambda \times 2\lambda$, indicating an excellent aperture efficiency. The results demonstrate that the designed array preserves the desired symmetry and exhibits a clean and well-focused main lobe.

The axial ratio (AR) performance is shown in Fig. 10 for $\phi = 0^\circ$. The AR remains well below 3 dB within the main beam, confirming the purity of the right-hand circular polarization (RHCP) in the broadside direction. The 3 dB axial-ratio beamwidth extends up to 49.7° , ensuring that the entire main lobe maintains satisfactory circular polarization performance, as required for LEO satellite communication links.

C. Digital beamforming and Coverage

Finally, Fig. 11 presents the digital beamforming results of the array. Three representative radiation patterns are shown: the main broadside beam and two additional beams corresponding to azimuth steering angles of $\pm 30^\circ$, which define the coverage limits of each face in the hexagonal pyramid configuration. The maximum directivity of the steered beams is 13.46 dBi, which corresponds to approximately 80% of the broadside directivity. The -3 dB beamwidth in these cases increases to 29.3° , providing sufficient overlap between adjacent faces to ensure continuous azimuthal coverage when the complete 3D antenna structure is assembled. Additionally, Fig. 12 illustrates the digital beamforming performance, showing two simultaneous beams steered in elevation at $\theta = \pm 15^\circ$ in a 3D representation.

IV. CONCLUSIONS

A planar 4×4 arrow-slot array with center microstrip feeding has been presented as a modular building block for space-based ADS-B reception. Circular polarization is achieved via sequential rotation with 90° element orientation and phase

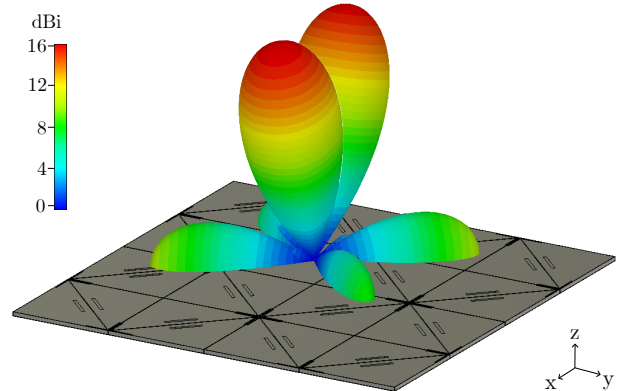


Fig. 12. Digital beamforming example with 2 beams at $\theta = \pm 15^\circ$, in the 4×4 array.

progression, while a hexagonal-pyramid assembly of identical subarrays offers continuous 360° azimuthal coverage with beams tilted toward Earth. Full-wave simulations indicate suitable input matching, controlled coupling, and stable patterns compatible with LEO payload constraints, making it a promising candidate for low-cost, high-performance, space-based ADS-B payloads in LEO orbit. Future work will address experimental validation and mechanical integration of the pyramid array in a CubeSat-class platform.

ACKNOWLEDGMENT

This research was conducted within the SATERA project, which has received funding from the SESAR 3 Joint Undertaking (JU) under grant agreement No. 101164313, with support from the European Union's Horizon Europe research and innovation programme and the SESAR 3 JU members other than the Union. Additional support was provided by Spain's Ministerio de Ciencia e Innovación under research projects PID2022-136869NB-C33, PID2022-141055NB-C21 and INDRA Espacio S.L.U. under the LINCE project of the Spanish Space Technology Program.

REFERENCES

- [1] J. Budroweit, F. Eichstaedt, and T. Delovski, "Aircraft surveillance from space: The future of air traffic control?: Space-based ads-b, status, challenges and opportunities," *IEEE Microwave Magazine*, vol. 25, no. 12, pp. 68–76, 2024.
- [2] SESAR 3 Joint Undertaking. (2024) *Space-based composite Ads-b and multilateration system validation through scalable simulations* [Online]. Available: <https://www.satera-sesar.eu/Informazioni/>. [Accessed: 01 October 2024].
- [3] H. Alshaer, A. Ganau, D. Brilhante, C. Cleary, M. A. Ullah, and V. Kramar, "Next-generation integrated communications, navigation, and surveillance services," in *2025 Integrated Communications, Navigation and Surveillance Conference (ICNS)*. IEEE, 2025, pp. 1–10.
- [4] A. Chesnitskiy, A. Kosmyrin, K. Kosmyrina, and K. Lemberg, "Design of a multibeam metasurface antenna for leo satellite communications payload," *Engineering Research Express*, vol. 4, no. 4, p. 045025, 2022.
- [5] G. Amendola, D. Cavallo, T. Chaloun, N. Defrance, G. Goussetis, M. Margalef-Rovira, E. Martini, O. Quevedo-Teruel, V. Valenta, N. J. Fonseca *et al.*, "Low-earth orbit user segment in the ku and ka-band: An overview of antennas and rf front-end technologies," *IEEE Microwave Magazine*, vol. 24, no. 2, pp. 32–48, 2023.

- [6] Y. Hu, Y. Lu, Q. You, K. Wang, Y. Wang, and J. Huang, "K-/ka-band dual-polarized differential series-fed waveguide slot array antenna with enhanced boresight radiation bandwidth," *IEEE Transactions on Antennas and Propagation*, 2024.
- [7] J. Vera-Sánchez, Á. Martín-Núñez, M. Ferrando-Rocher, and M. Ferrando-Bataller, "Circularly polarized conical array for ads-b applications in leo satellites," in *2025 19th European Conference on Antennas and Propagation (EuCAP)*. IEEE, 2025, pp. 1–3.
- [8] J. Vera-Sánchez, M. Ferrando-Rocher, G. Casasus-Goyeneche, and M. Ferrando-Bataller, "L-band unit-cell antenna design for satellite-based ads-b surveillance," in *2025 IEEE International Symposium on Antennas & Propagation and North American Radio Science Meeting (IEEE AP-S/URSI)*, 2025.
- [9] M. Leonardi, M. Mohebbi, and G. Sidoretti, "Robust and resilient gnss synchronization of leo satellites for space-based aircraft multilateration," in *2025 IEEE 12th International Workshop on Metrology for AeroSpace (MetroAeroSpace)*, 2025, pp. 654–659.
- [10] M. Leonardi, G. Sidoretti, E. Navarra, and M. Mohebbi, "Space-based multilateration system for a gnss-independent aircraft localisation," in *76th International Astronautical Congress (IAC)*, 2025.